Supporting Information

Aerobic Oxidation of Aldehydes into Acid in Water with Catalytic Carbene Copper under Neutral Conditions

Songbo Xu,[c] Xiaomin Zhang,[a,b,] Wenjie Xiong,[a] Ping Li,[a] Wentao Ma,[a] Xingbang Hu,[a,b,*] and Youting Wu[a,b,*]*

[a] Key Laboratory of Mesoscopic Chemistry of MOE, School of Chemistry and Chemical Engineering, Nanjing University, 163 Xianlin Road, Qixia District, Nanjing 210023, People's Republic of China

[b] Yuxiu Postdoctoral Institute, Nanjing University, Nanjing 210023, PR China

[c] Shandong Kanbo Biochemical Technology Co., Ltd., Dongying, 257400, P. R. China

E-mail: xmzhang@nju.edu.cn;huxb@nju.edu.cn; ytwu@nju.edu.cn

EXPERIMENTAL

General Information

4-chlorobenzaldehyde, p-methyl benzaldehyde, o-tolualdehyde, m-tolualdehyde, 2-bromobenzaldehyde, 3-bromobenzaldehyde, 4-bromobenzaldehyde, and p-fluorobenzaldehyde were purchased from Aladdin (Shanghai, China). Other chemicals were supplied by Energy Chemical. All chemicals were of analytical grade and used as received without any further purification. ^{1}H NMR and ^{13}C NMR spectrum were recorded on a Bruker Avance-400 instrument, 400 MHz for ^{1}H NMR and 100 MHz for ^{13}C NMR, with $CDCl_3$ or DMSO-d_6 as solvent throughout all cases. All chemical shifts were quoted in parts per million (ppm) and reported relative to an internal

tetramethylsilane standard. The yields were determined using a Shimadzu GC2014 gas chromatograph with a flame-ionization detector.

Synthesis and Characterization of Catalyst

The synthesis procedure can be referred to our previous work. Briefly, diethyl cyclic iminium tetrafluoroborate salt (2.0 g), potassium bis(trimethylsilyl)amide (KHMDS, 1.0 g), and copper(I) chloride (CuCl, 0.5 g) were loaded in a Schlenk tube under nitrogen protection with a purity of 99.999%. THF (50 mL) was injected to the solids at -78 °C and the mixture was stirred for 1 h at the same temperature. The mixture was warmed slowly to room temperature, followed by stirring for another 8h. The volatiles were removed under vacuum and the residue was washed with hexanes (50 mL). After removing the volatiles, the residue was extracted with benzene (60 mL). The solution was evaporated and dried under vacuum, affording product as a white solid (71% yield).

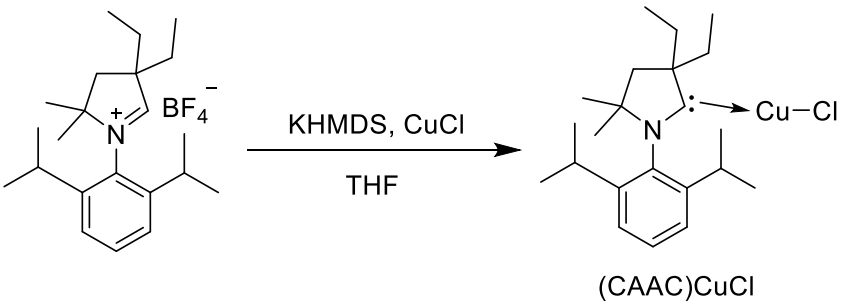

Scheme S1. The schematic diagram of the synthesis (CAAC)CuCl.

The characterization data of catalyst can be found as follows:

HRMS (m/z): $[M+K]^+$ calcd for $[C_{22}H_{35}NCuCl\cdot K]^+$, 450.14; found, 450.15.; Elemental Analysis: C, 64.05%; H, 8.55%; N, 3.40%; found: C, 62.85%; H, 8.97%; N, 3.58%.

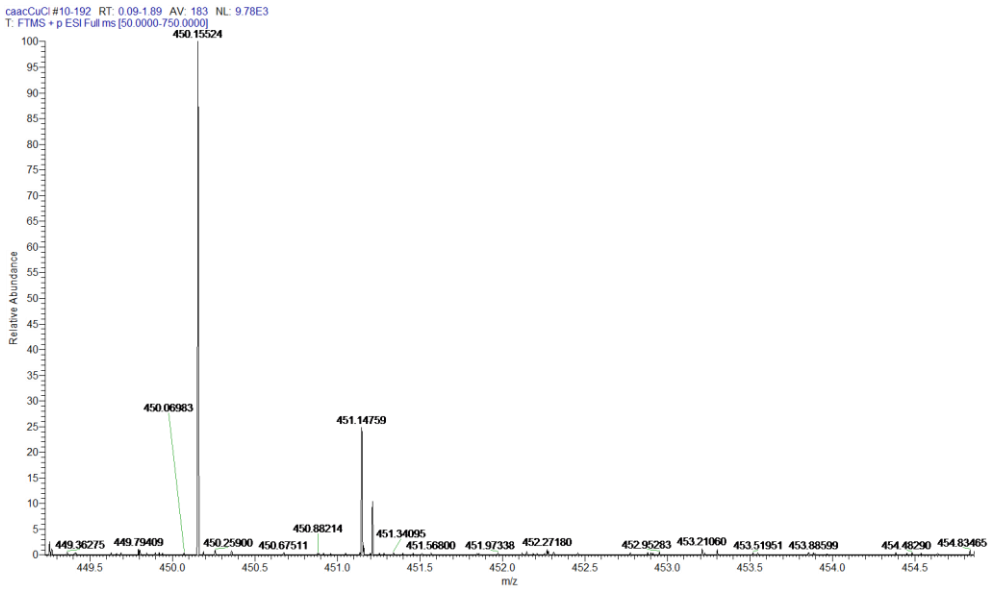

Figure S1. ESI-MS of (CAAC)CuCl.

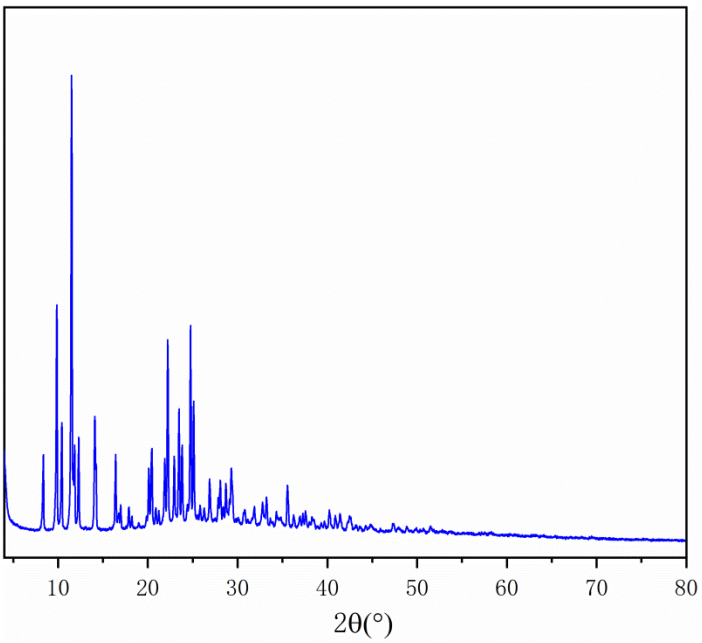

Figure S2. PXRD of (CAAC)CuCl.

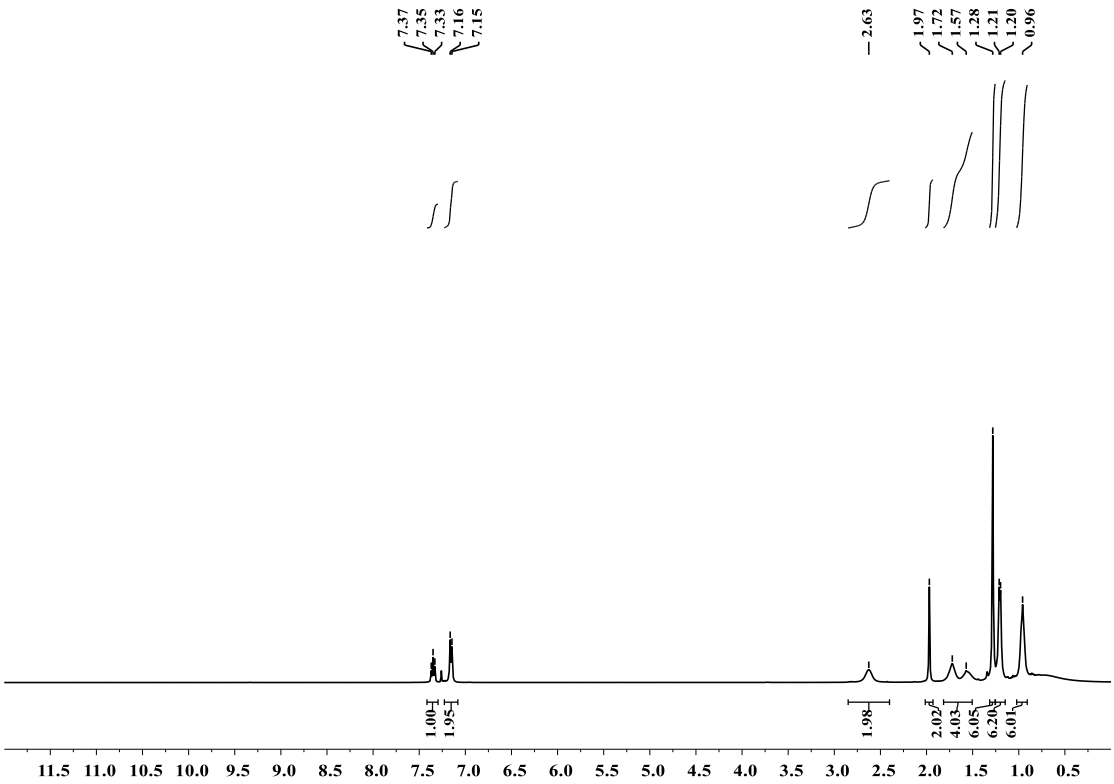

Figure S3. ^{1}H NMR spectra of (CAAC)CuCl.

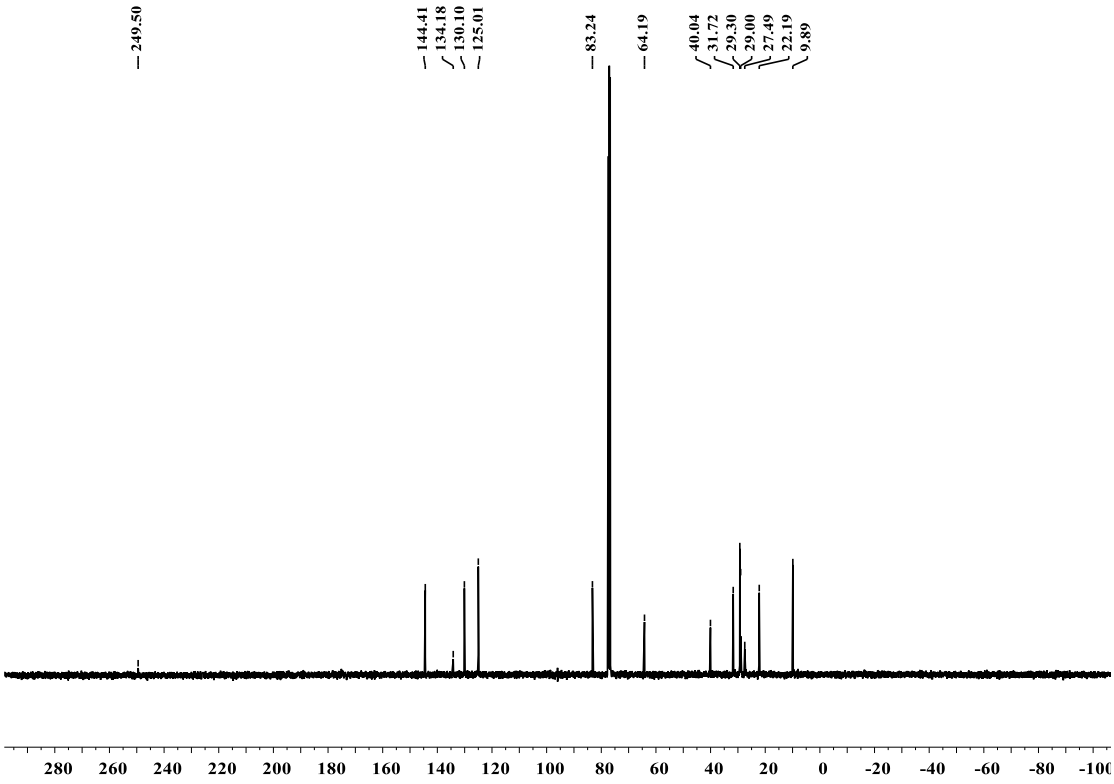

Figure S4. ^{13}C NMR spectra of (CAAC)CuCl.

General procedures oxidation of aldehydes using O_2 as the oxidant

A closed reaction vessel, charged with water 40 mL, aldehyde was introduced to form a final concentration. Oxygen was simply flushed into the vessel and sealed with a balloon filled with enough oxygen. The reaction mixture was stirred for 24 h at 25 °C. Isolation of the product from the system was quite easy: after reaction, enough sodium hydroxide was added in the mixture to offer a homogeneous solution. Then, dichloromethane (3 × 2 ml) were used to extract the unreacted aldehydes. Excess diluted HCl were added in the aqueous solution to make the pH value of 2. Then, the product was isolated by extraction into ethyl ether followed by the removal of solvent under reduced pressure at RT. After reaction completed, yields were analyzed by GC with biphenyl as the internal standard.

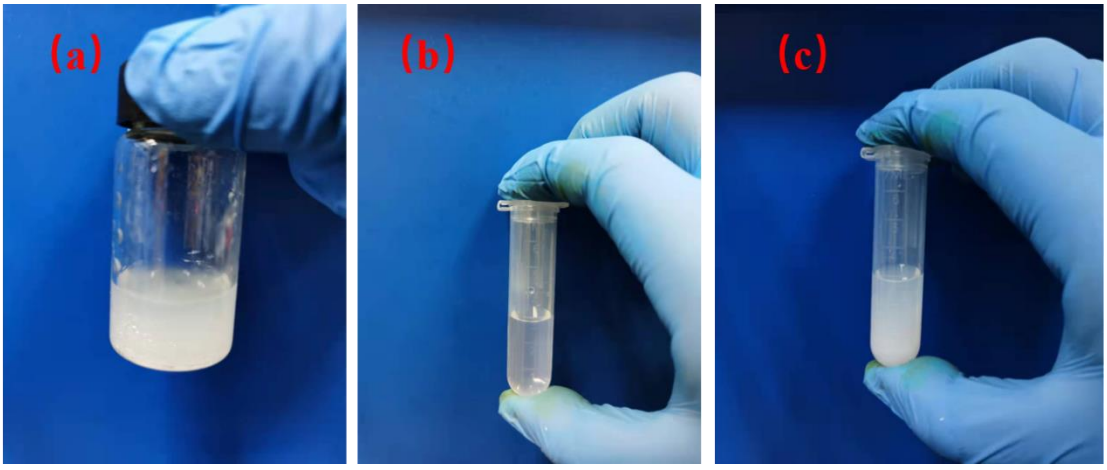

Figure S5. (a) The reaction system under going; (b) Upper clear solution of reaction system after centrifugation; (c) After the addition $AgNO_3/HNO_3$ (a.q.) into upper clear solution.

Theoretical calculation method

All the geometries were fully optimized with Gaussian 09 program using B3LYP method based on density functional theory [S1]. LANL2DZ basis set was used for Cu and 6-311+G* basis set for other atoms. Energy calculations as well as Zero-point energies (ZPE) correction have been performed at the same theory. All energies reported in this work are corrected by ZPE. The computed stationary points have been characterized as minima or transition states by diagonalizing the Hessian matrix and analyzing the vibrational normal modes. In this way, the stationary points can be classified as minima if no imaginary frequencies are shown or as transition states if only one imaginary frequency is obtained. The particular nature of the transition states has been determined by analyzing the motion described by the eigenvector associated with the imaginary frequency.

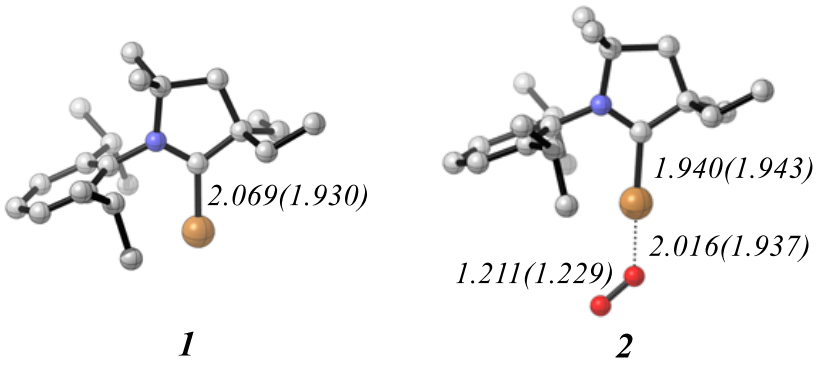

Figure S6. The optimized structure of (CAAC)Cu (1) and (CAAC)Cu-O_2 (2). The shown values are bond length (in Å) of high (low) spin state structures.

Characterization data for all products.

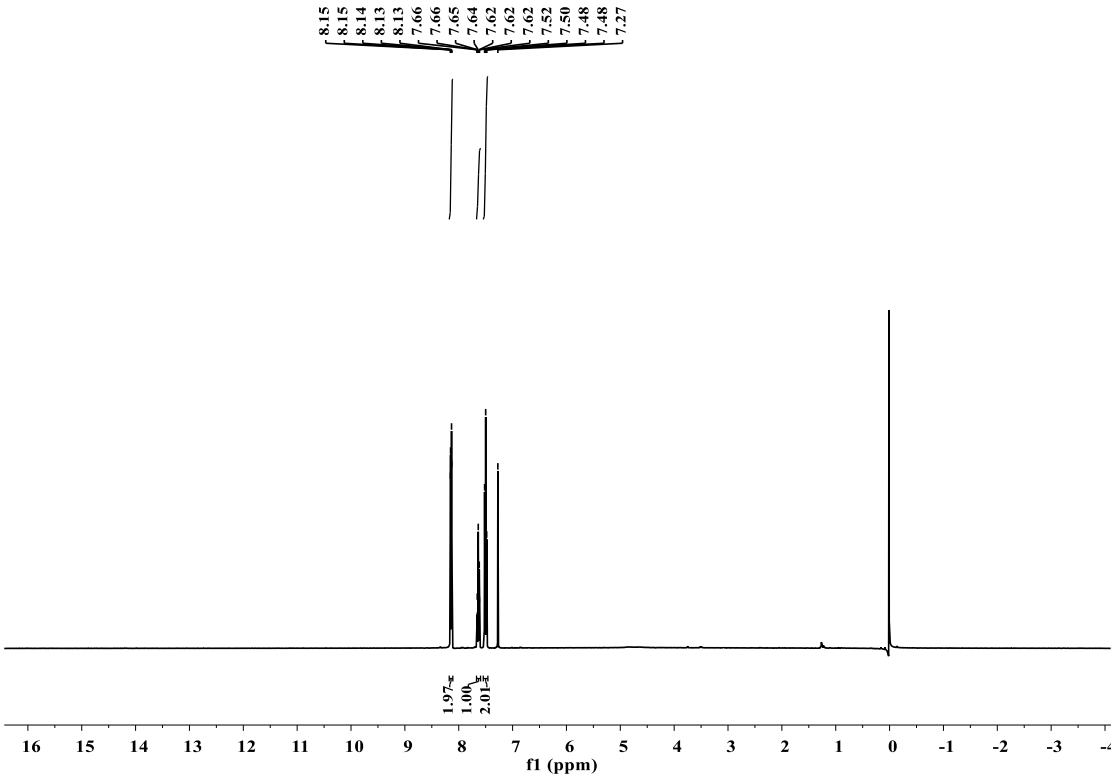

Figure S7. ^{1}H NMR spectra of benzoic acid.

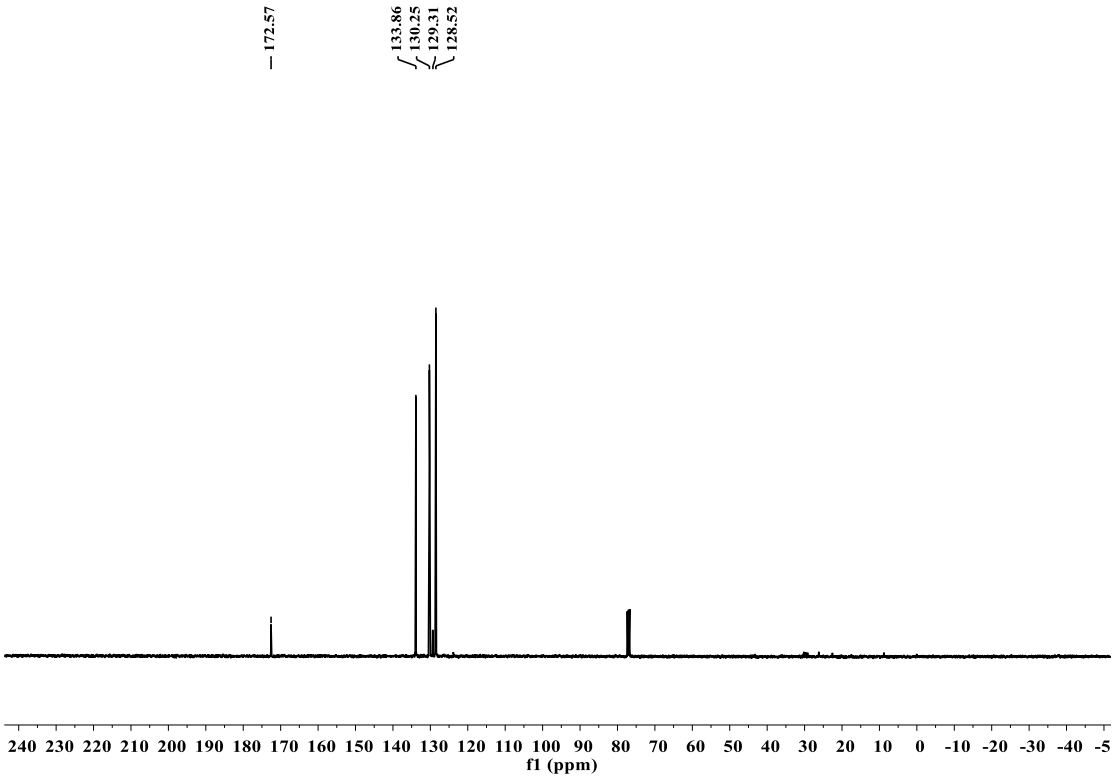

Figure S8. ^{13}C NMR spectra of benzoic acid.

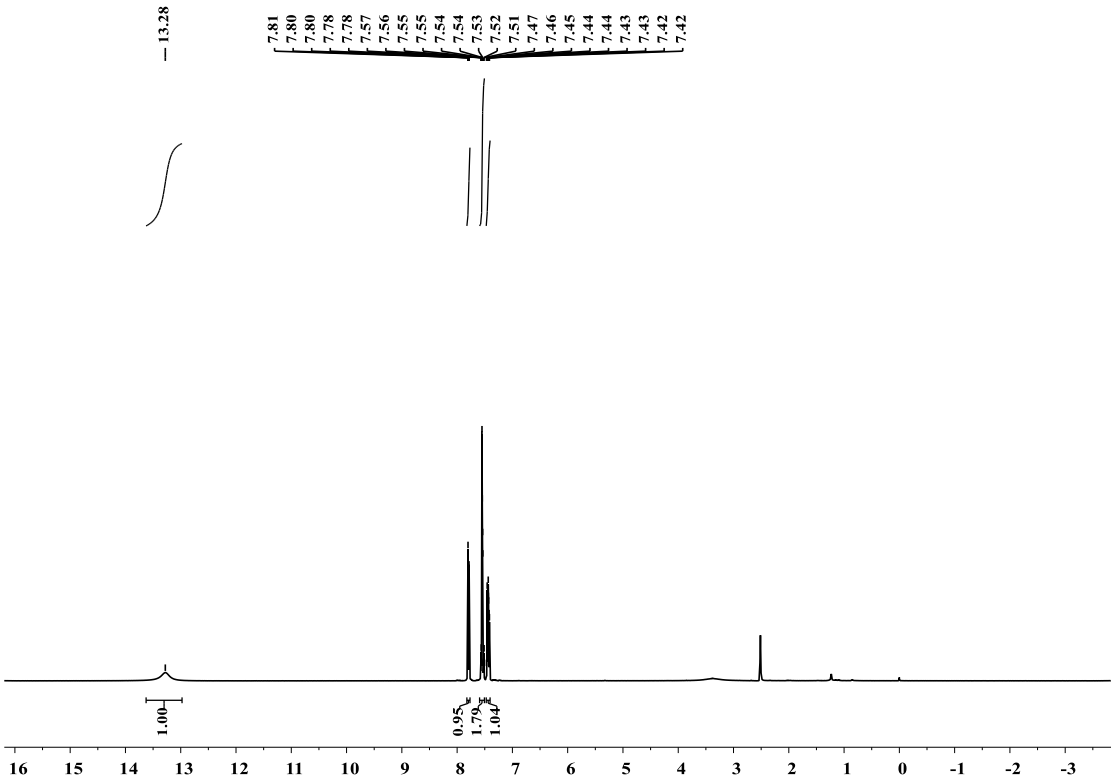

Figure S9. ^{1}H NMR spectra of o-chlorobenzoic acid.

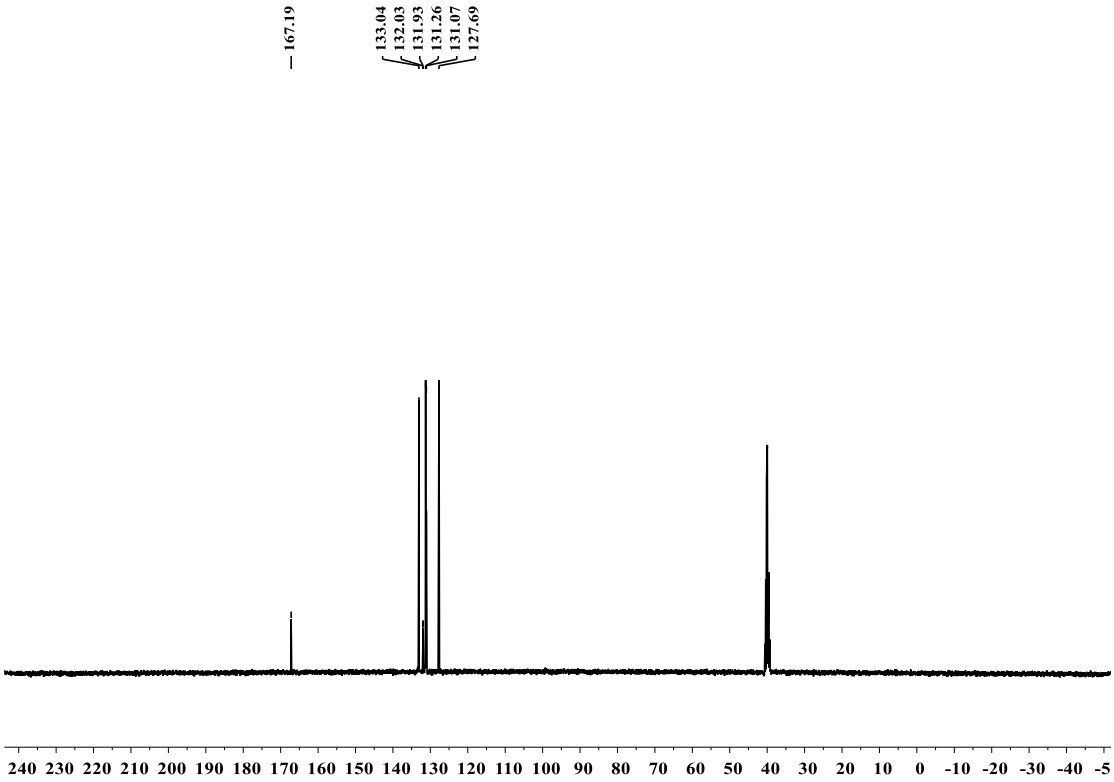

Figure S10. ^{13}C NMR spectra of o-chlorobenzoic acid.

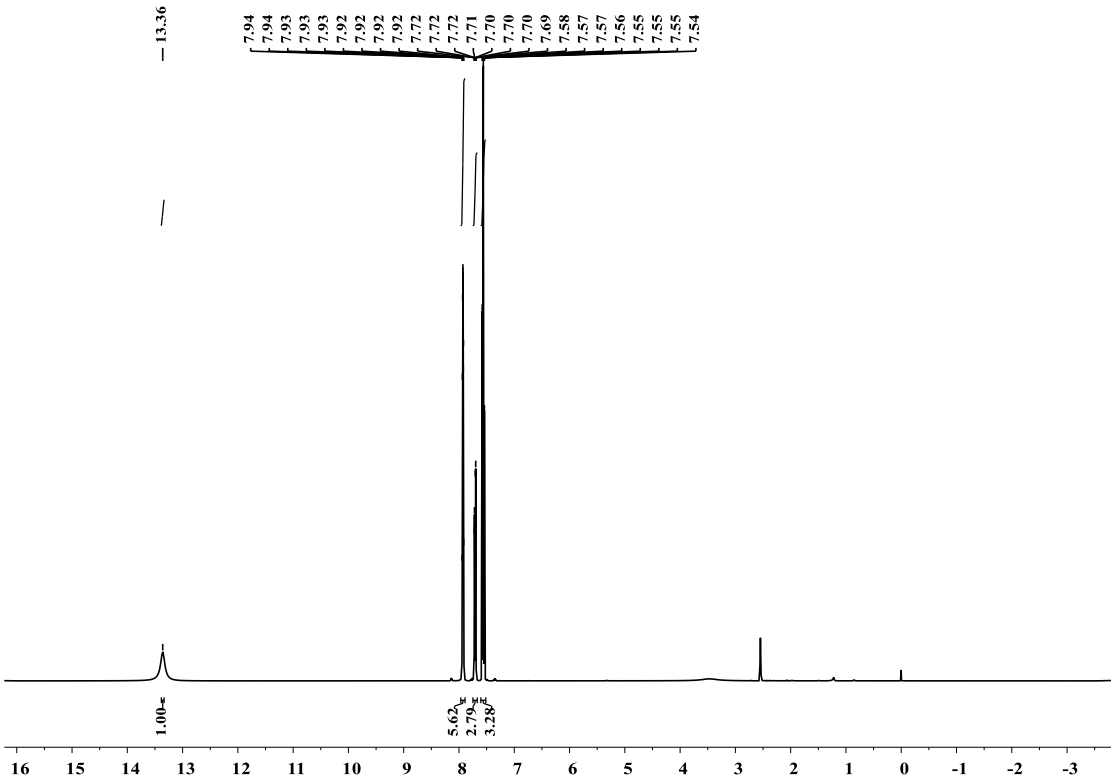

Figure S11. ^{1}H NMR spectra of m-chlorobenzoic acid.

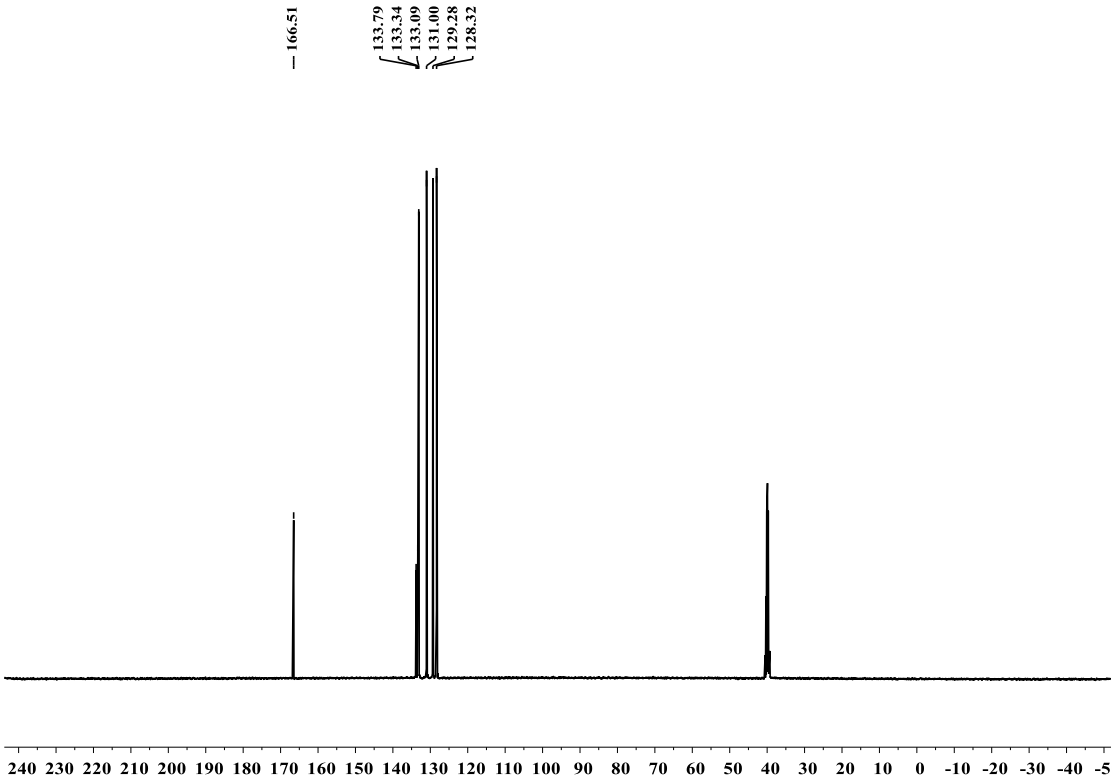

Figure S12. ^{13}C NMR spectra of m-chlorobenzoic acid.

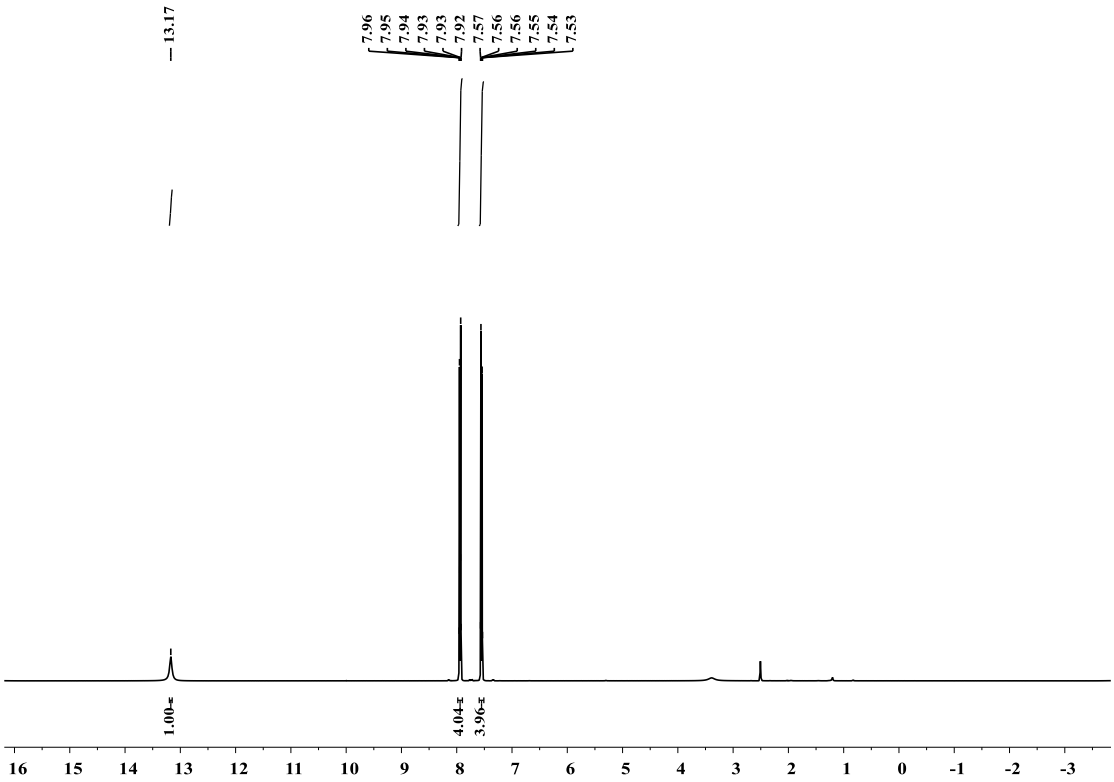

Figure S13. ^{1}H NMR spectra of p-chlorobenzoic acid.

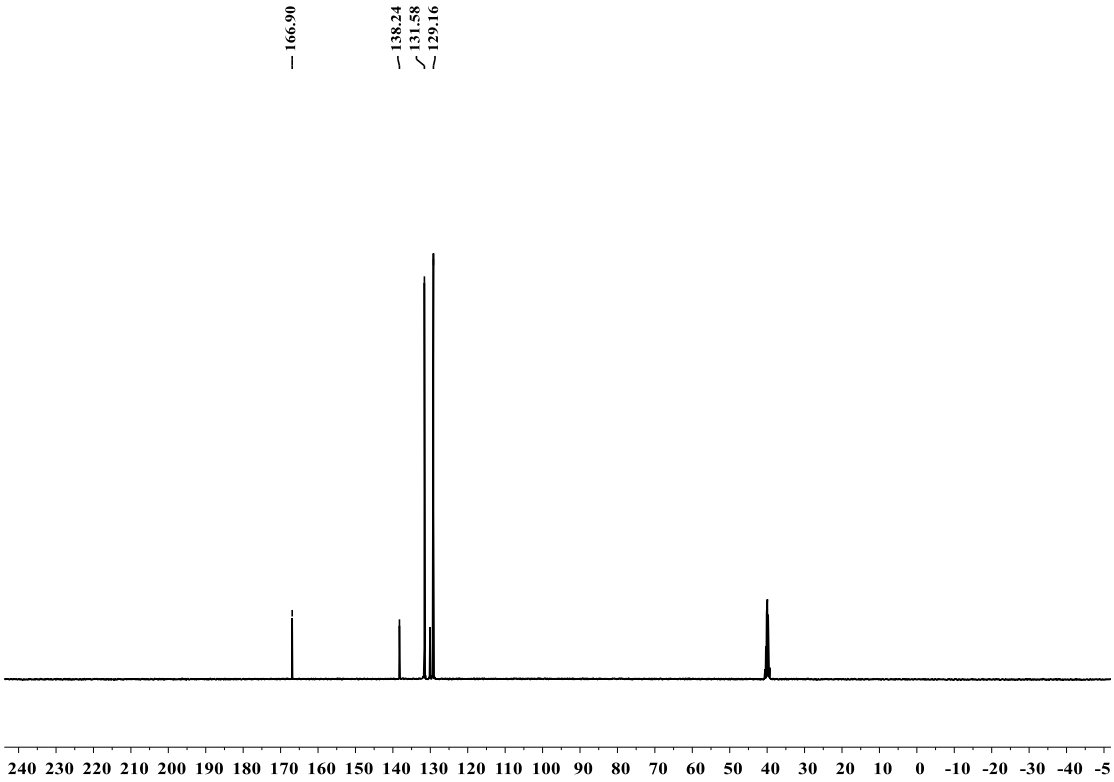

Figure S14. ^{13}C NMR spectra of p-chlorobenzoic acid.

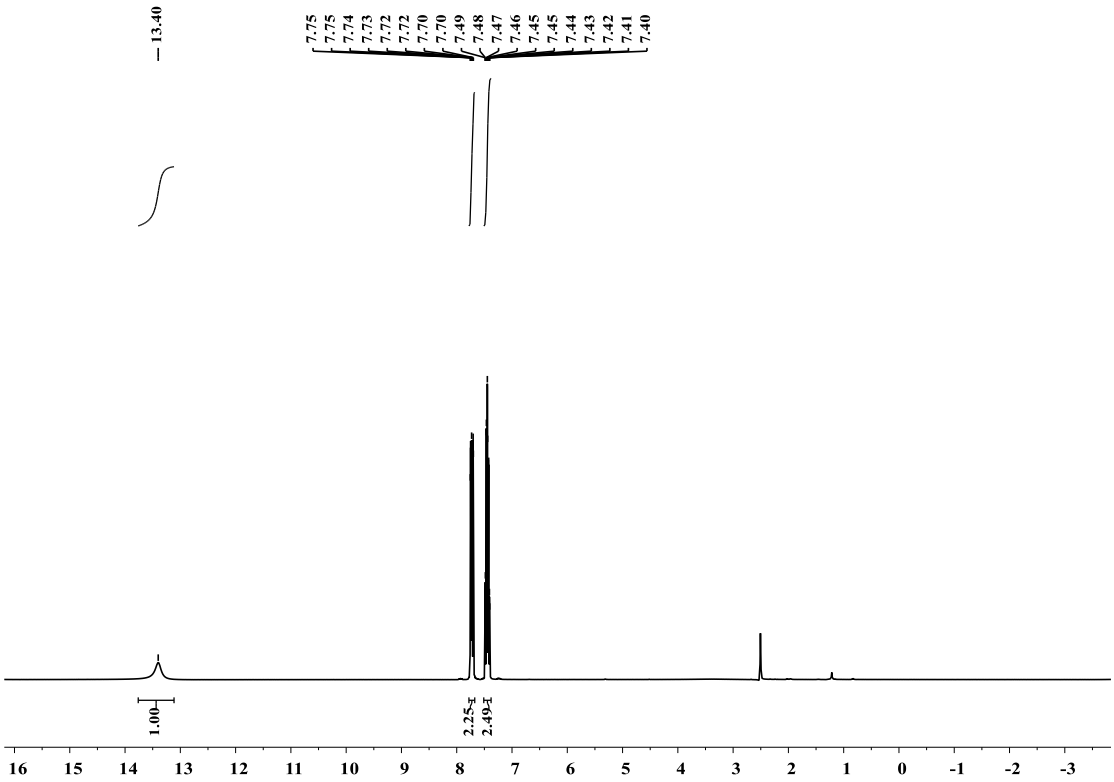

Figure S15. ^{1}H NMR spectra of 2-bromobenzoic acid.

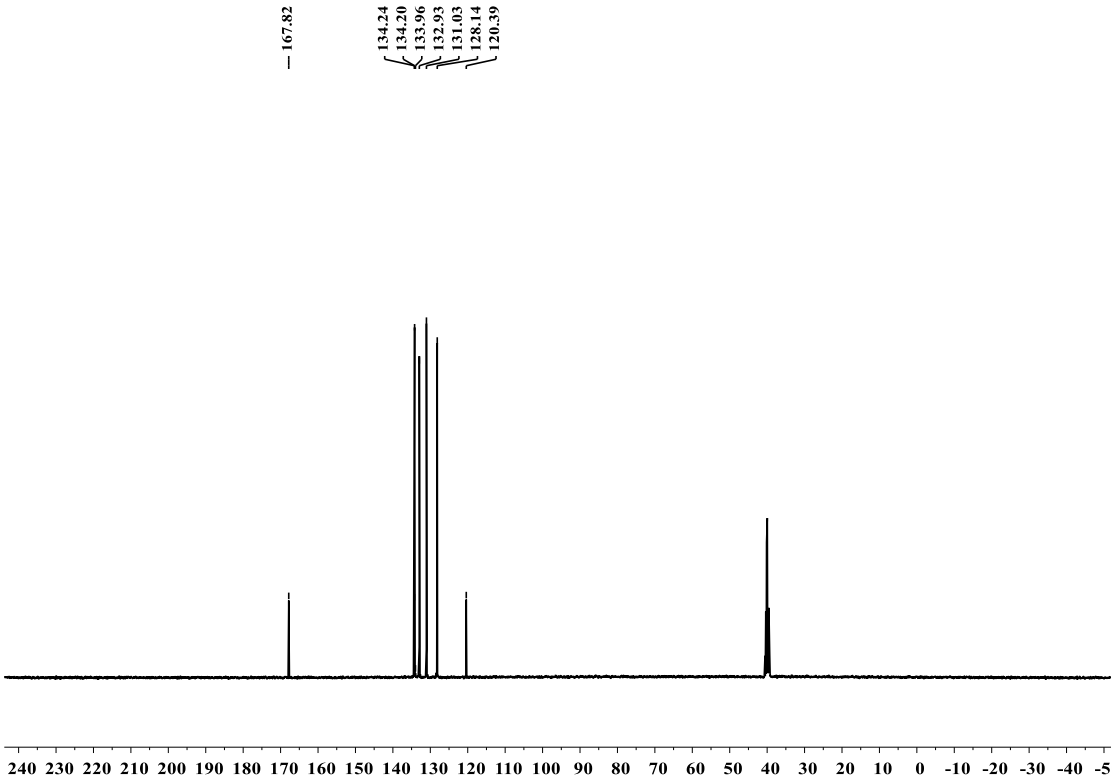

Figure S16. ^{13}C NMR spectra of 2-bromobenzoic acid.

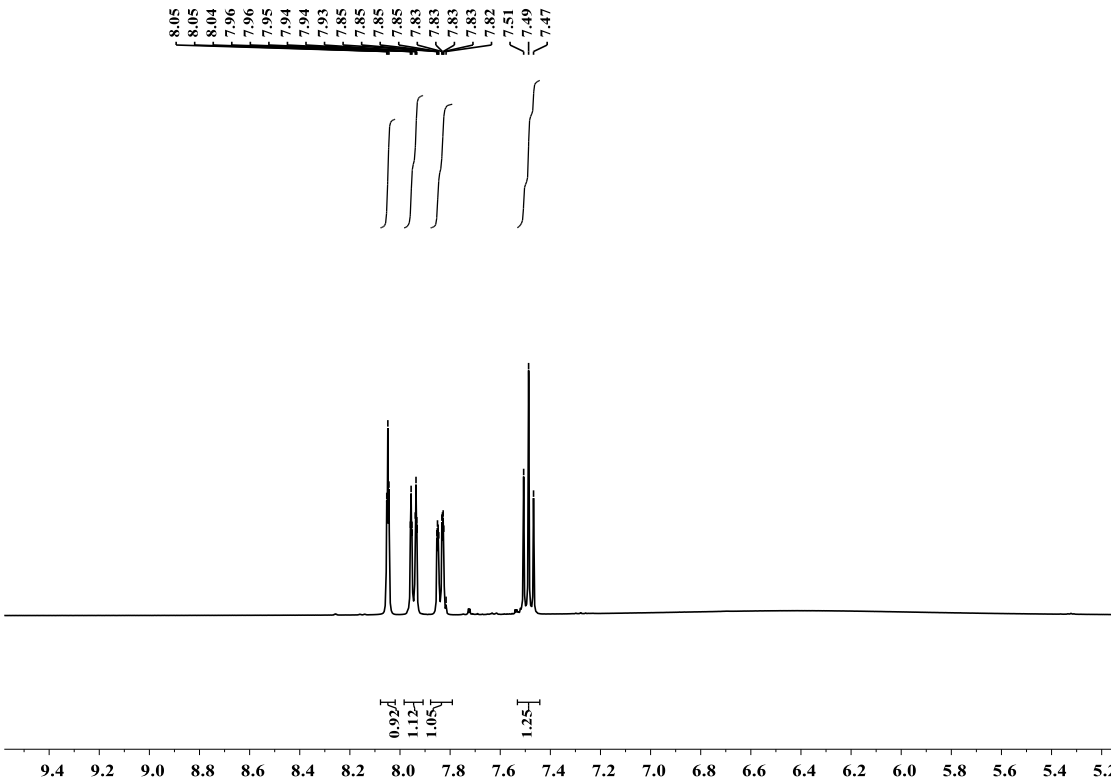

Figure S17. ^{1}H NMR spectra of 3-bromobenzoic acid.

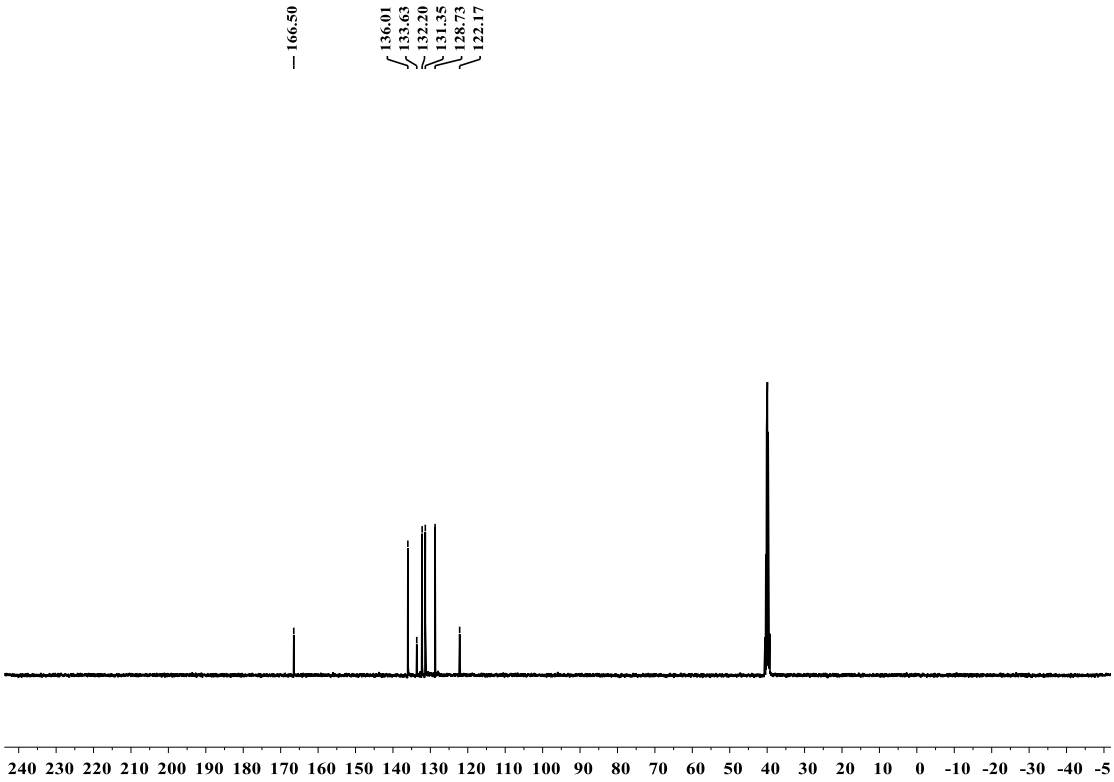

Figure S18. ^{13}C NMR spectra of 3-bromobenzoic acid.

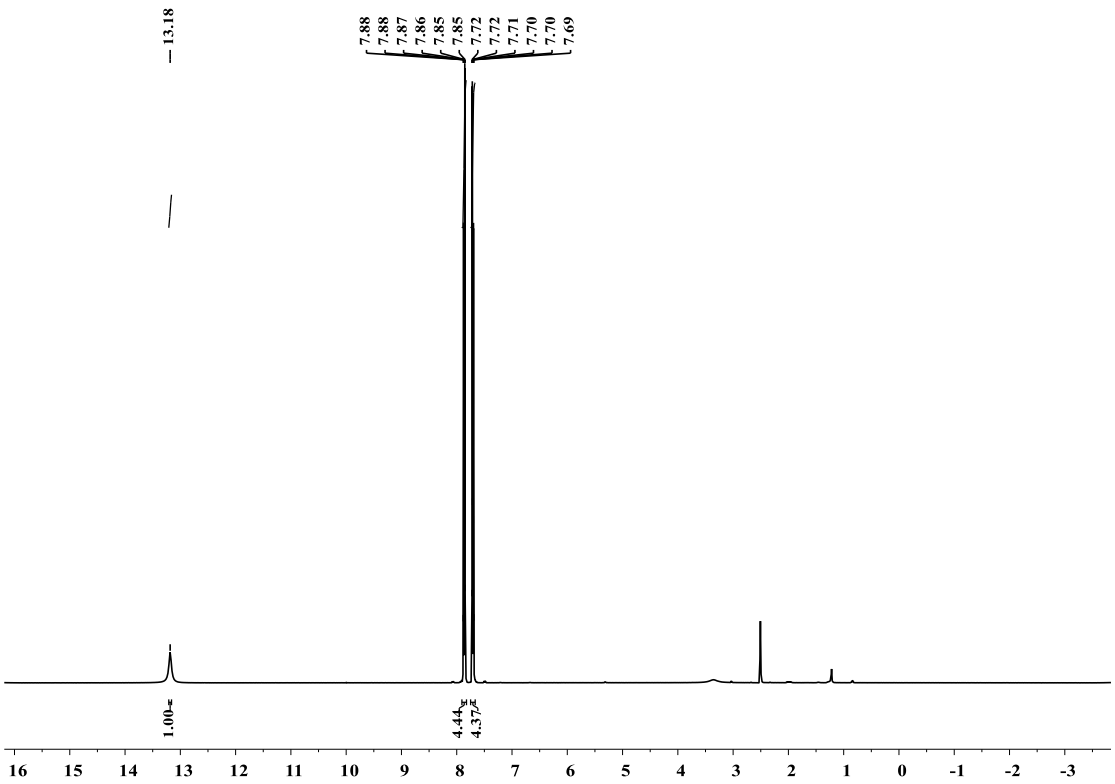

Figure S19. ^{1}H NMR spectra of 4-bromobenzoic acid.

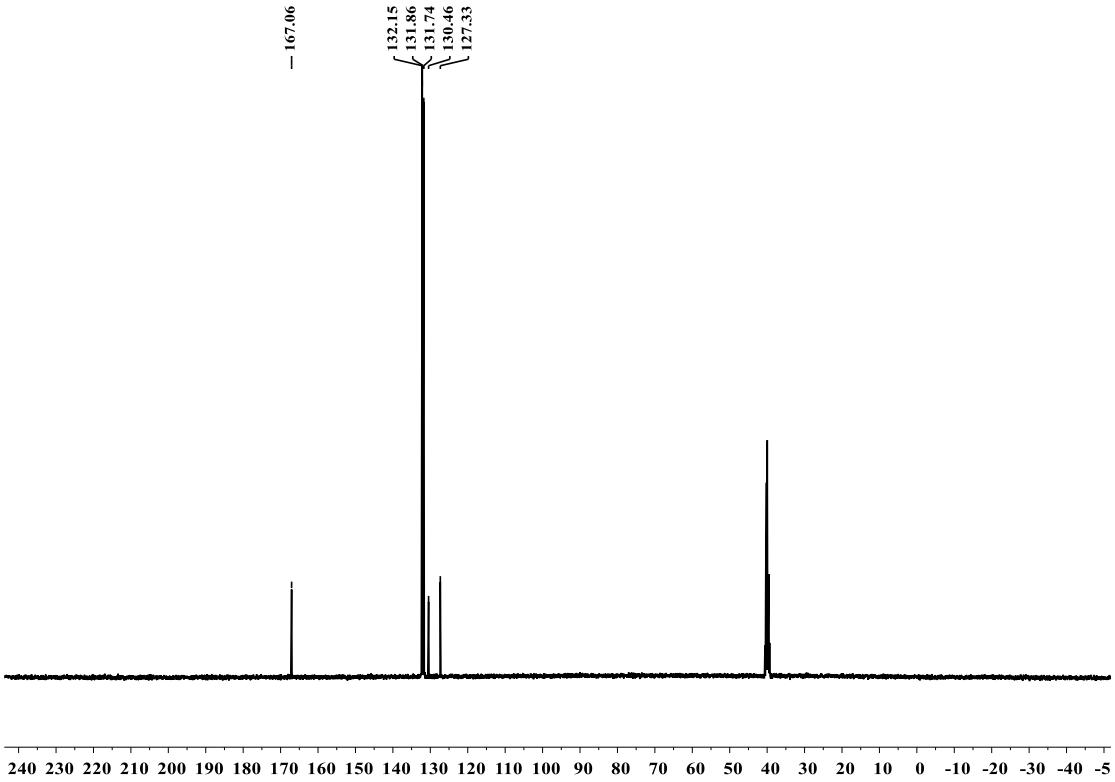

Figure S20. ^{13}C NMR spectra of 4-bromobenzoic acid.

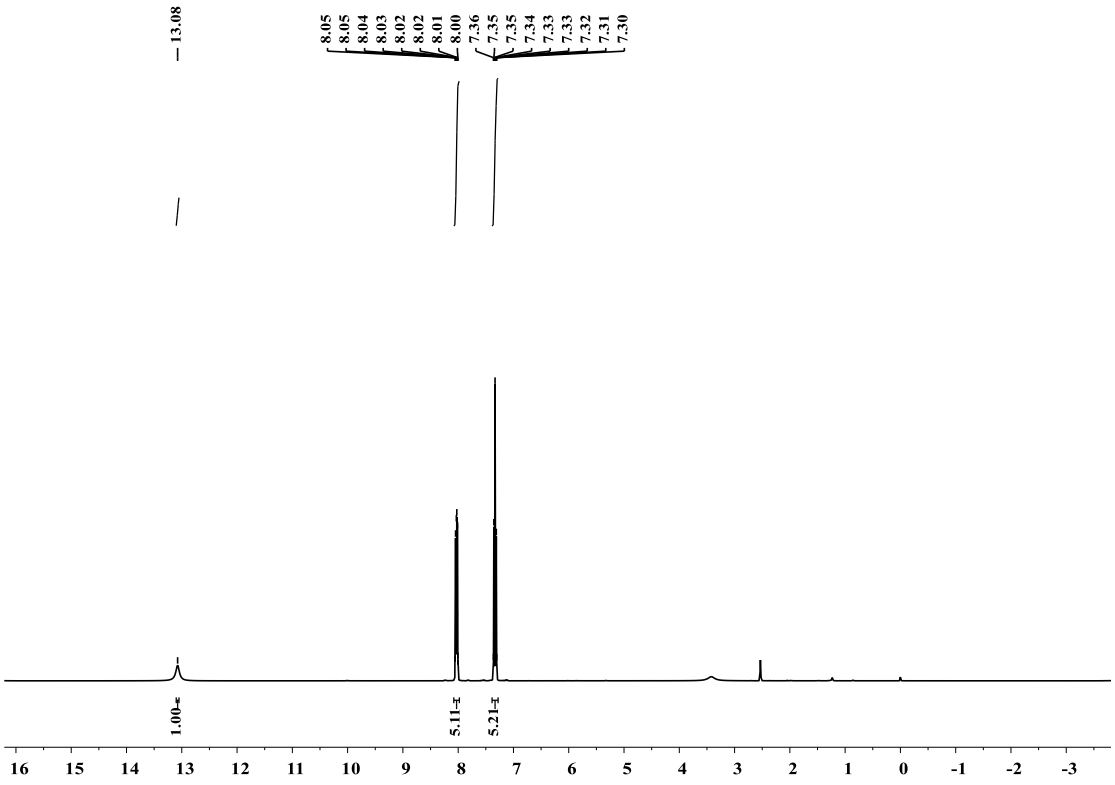

Figure S21. ^{1}H NMR spectra of 4-fluorobenzoic acid.

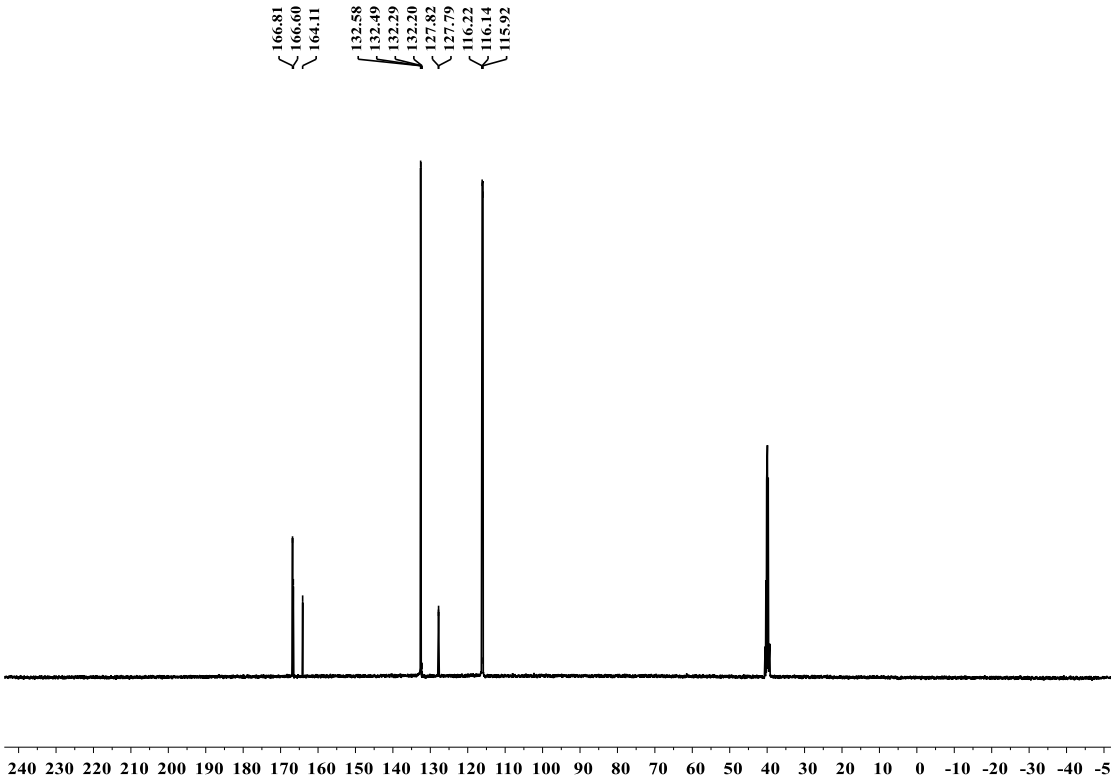

Figure S22. ^{13}C NMR spectra of 4-fluorobenzoic acid.

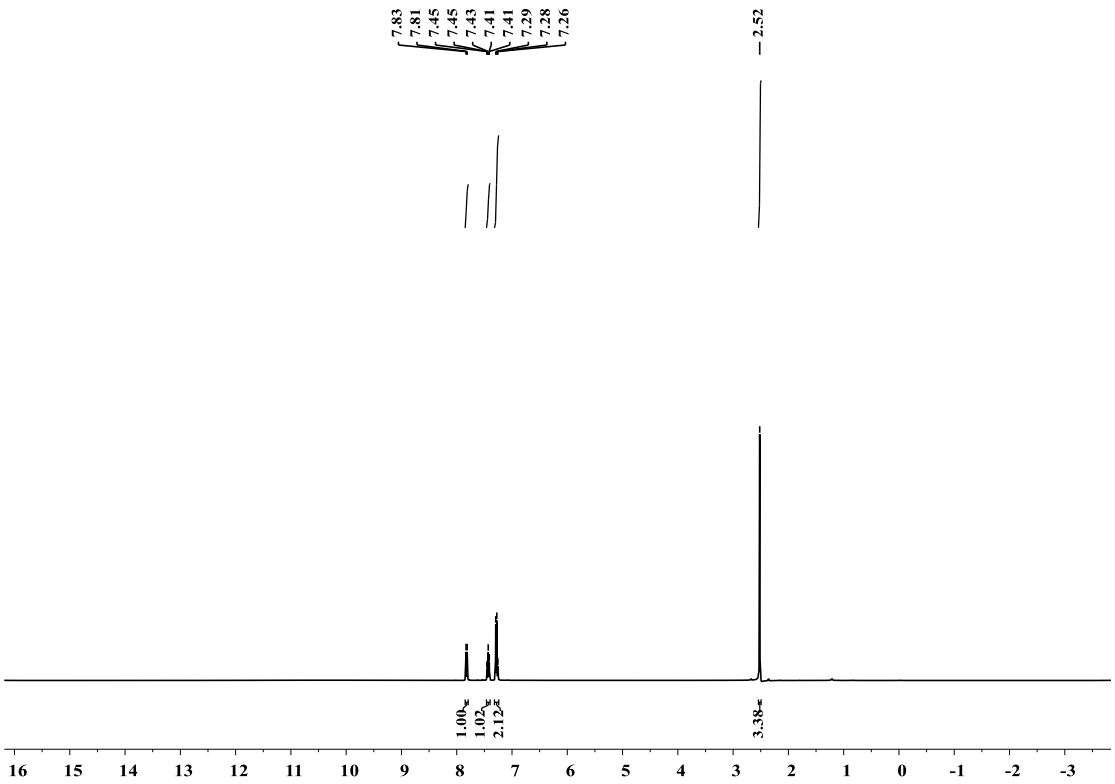

Figure S23. ^{1}H NMR spectra of o-toluic acid.

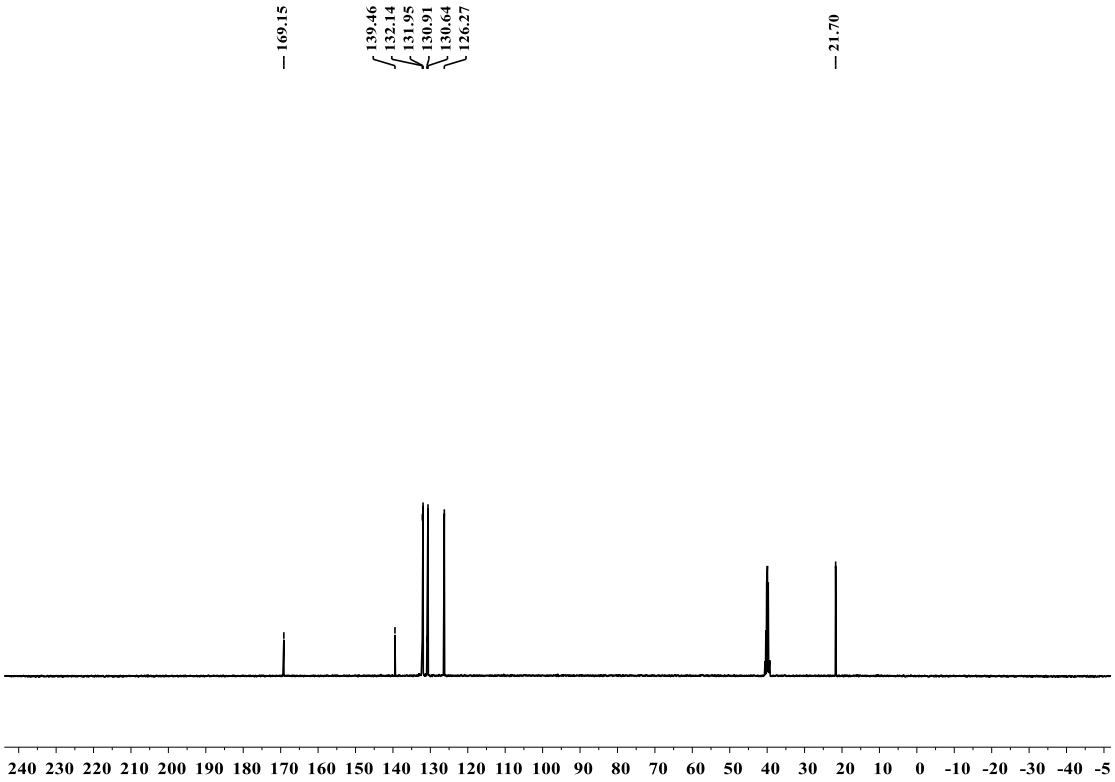

Figure S24. ^{13}C NMR spectra of o-toluic acid.

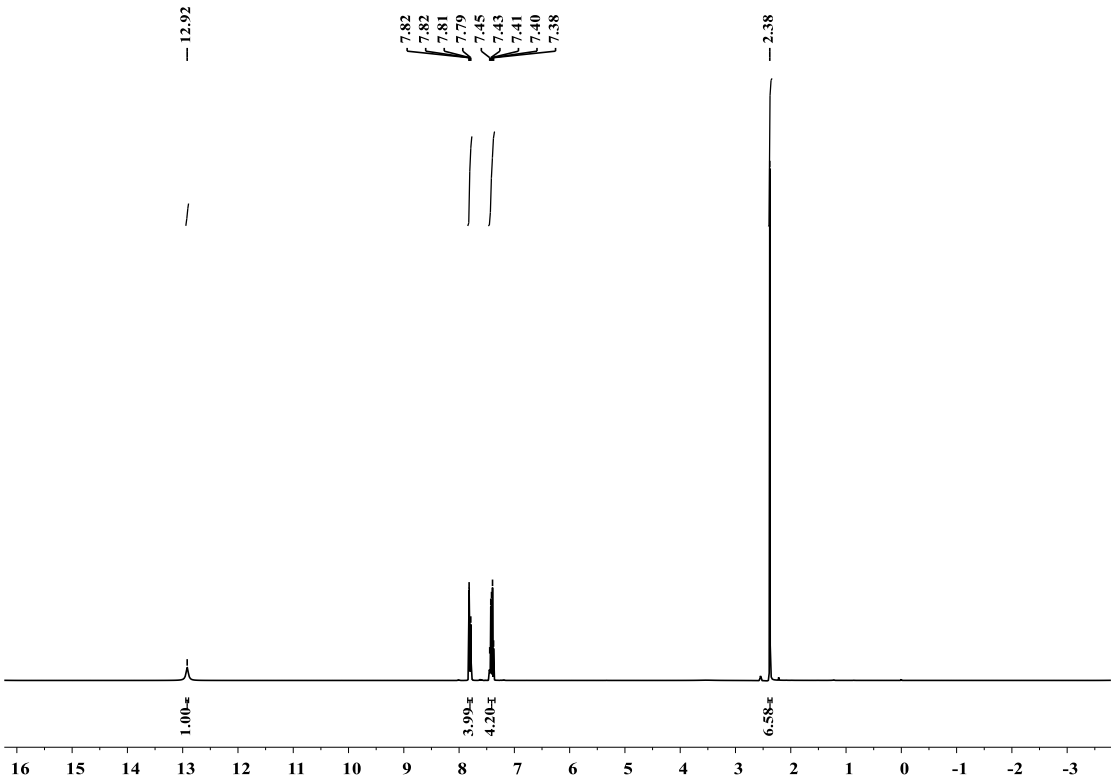

Figure S25. ^{1}H NMR spectra of m-toluic acid.

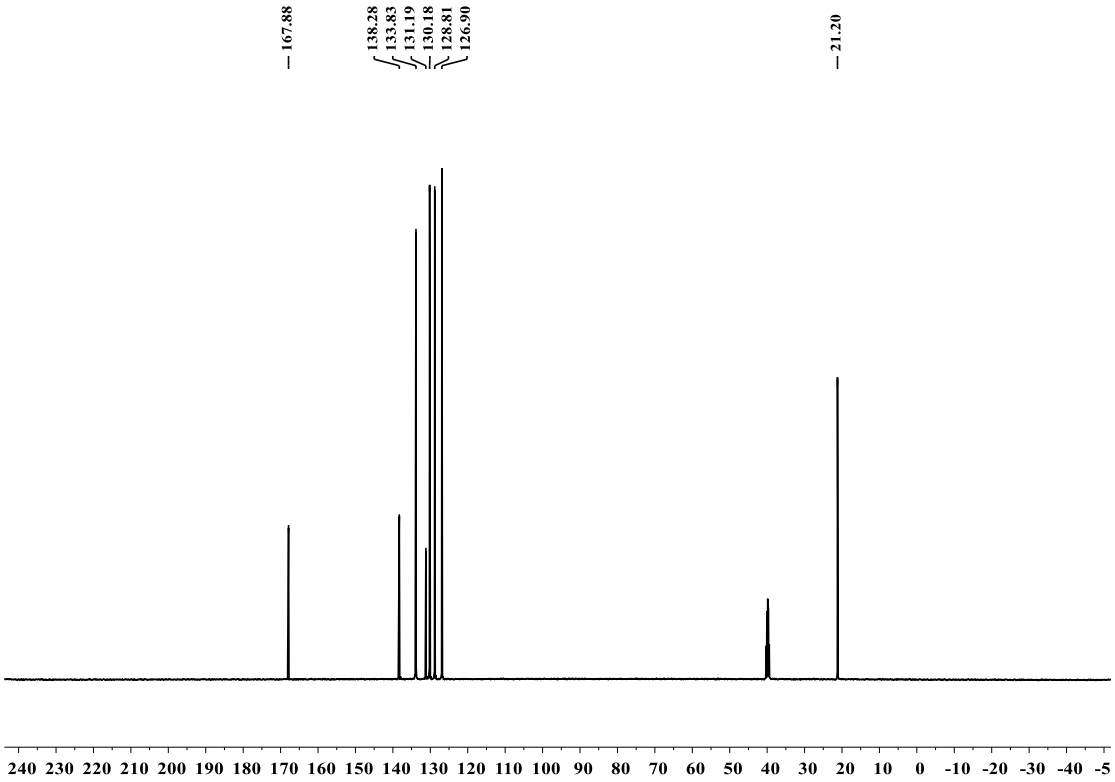

Figure S26. ^{13}C NMR spectra of m-toluic acid.

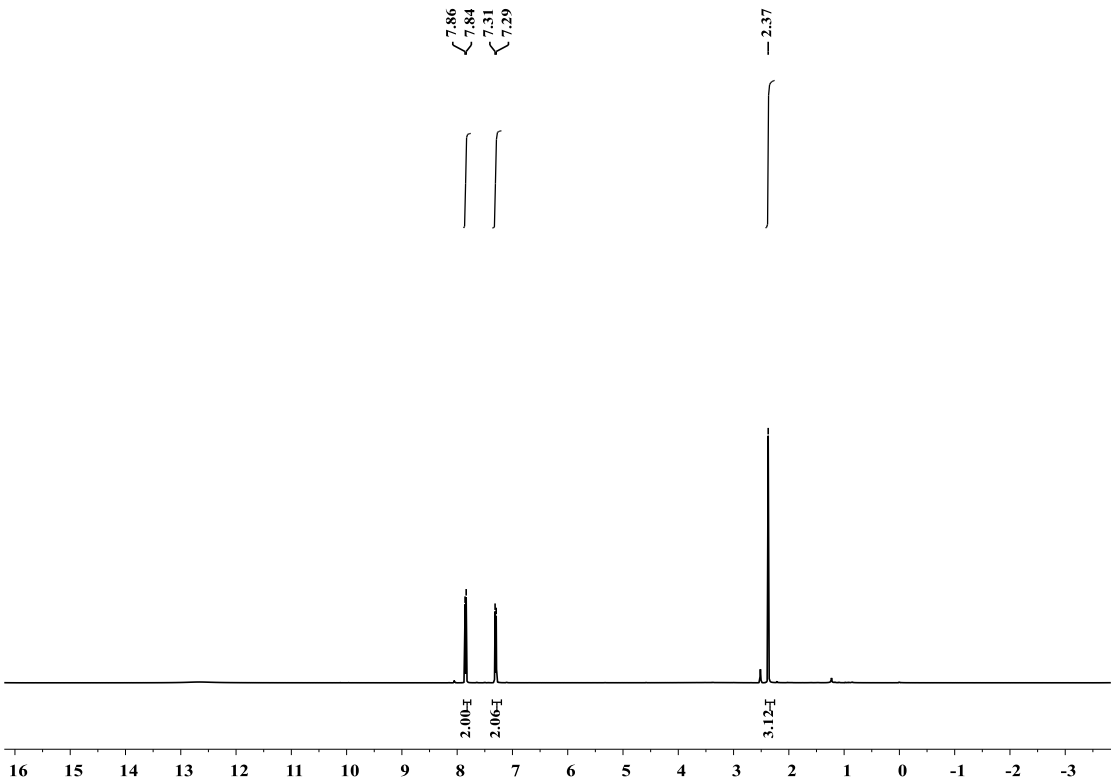

Figure S27. ^{1}H NMR spectra of p-toluic acid.

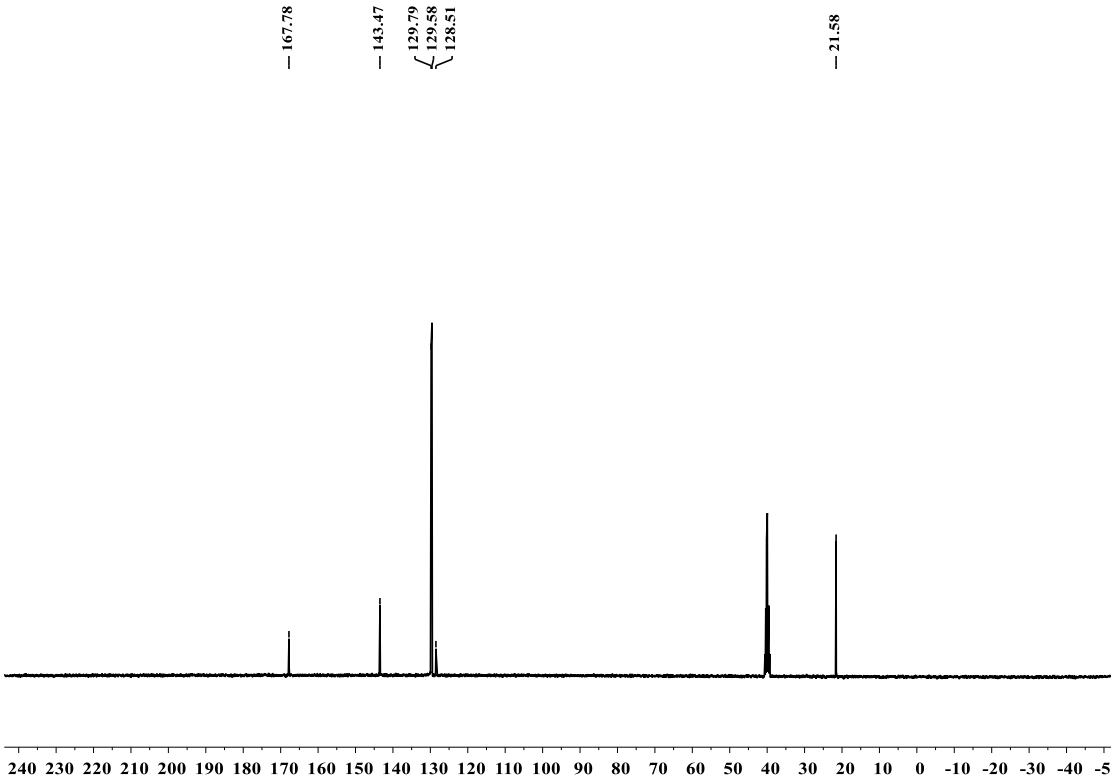

Figure S28. ^{13}C NMR spectra of p-toluic acid.

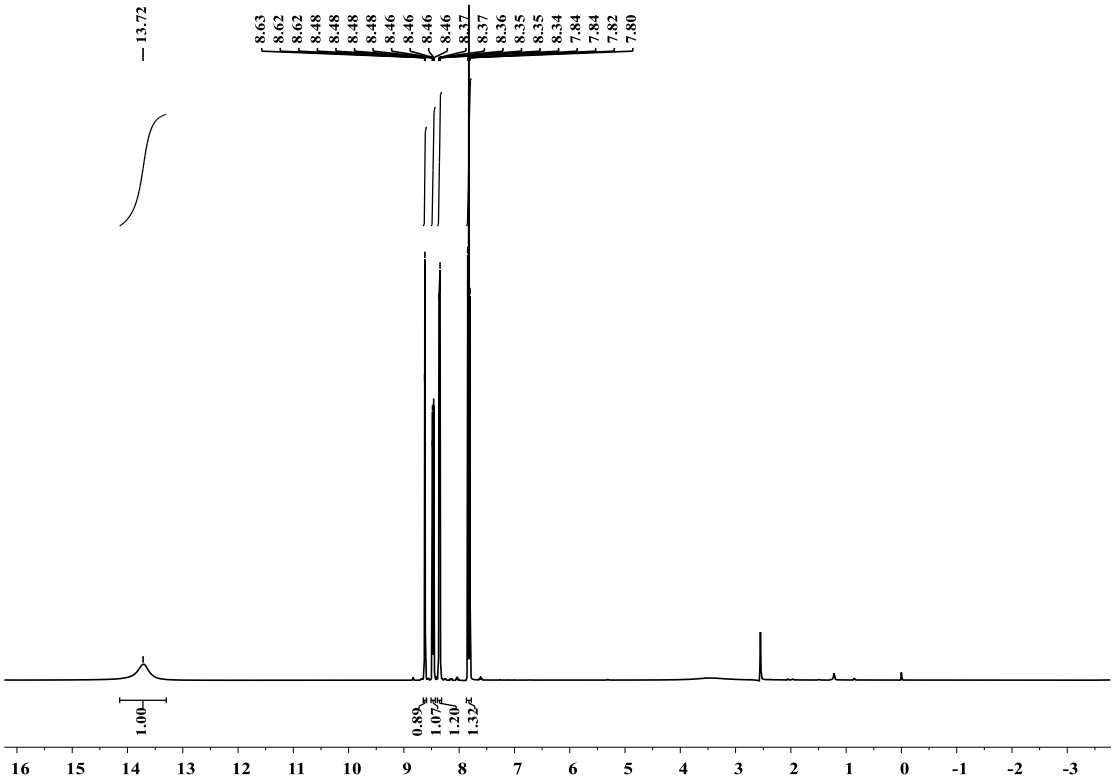

Figure S29. ^{1}H NMR spectra of m-nitrobenzoic acid.

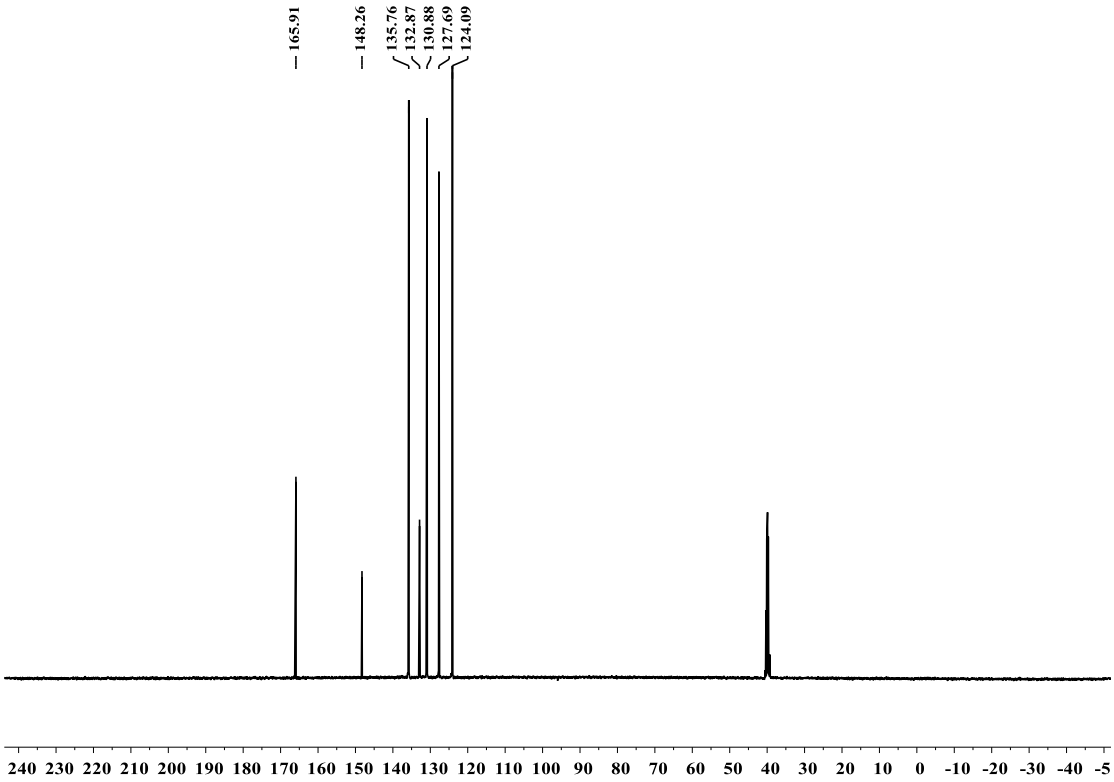

Figure S30. ^{13}C NMR spectra of m-nitrobenzoic acid.

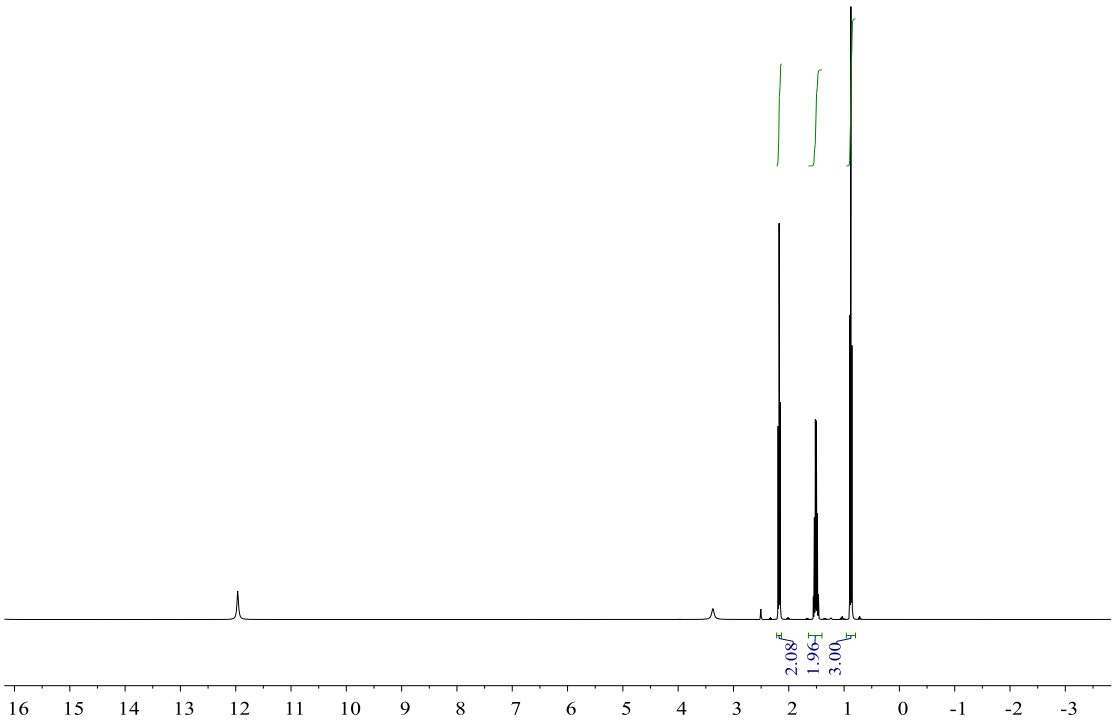

Figure S31. ^{1}H NMR spectra of butyric acid.

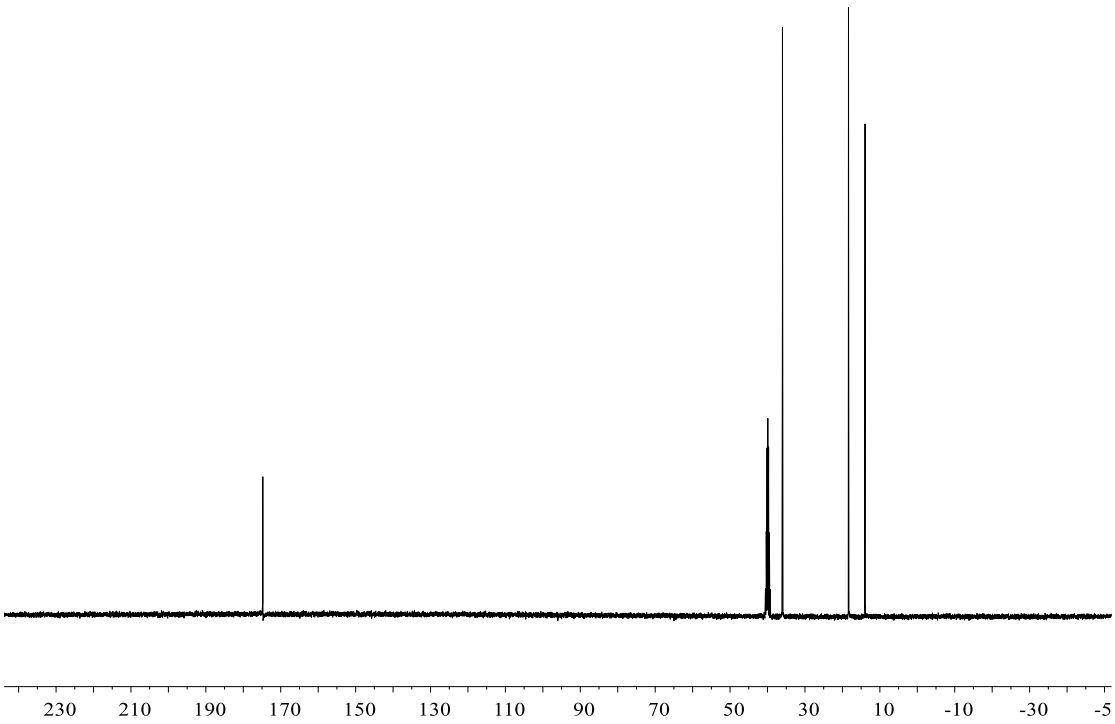

Figure S32. ^{13}C NMR spectra of butyric acid.

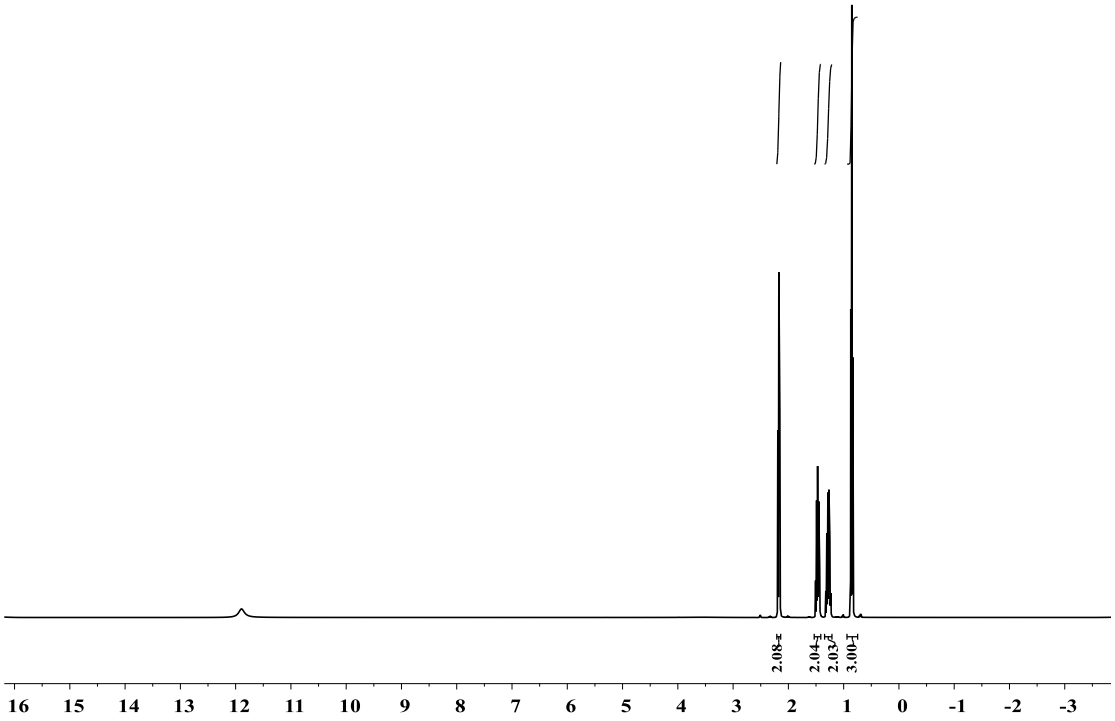

Figure S33. ^{1}H NMR spectra of valeric acid.

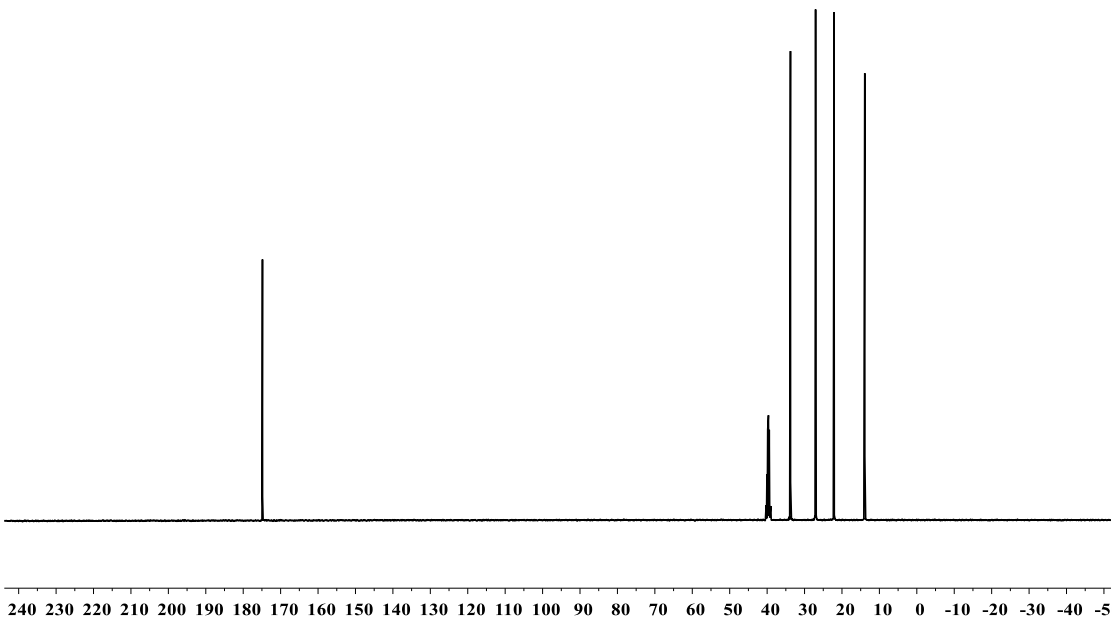

Figure S34. ^{13}C NMR spectra of valeric acid.

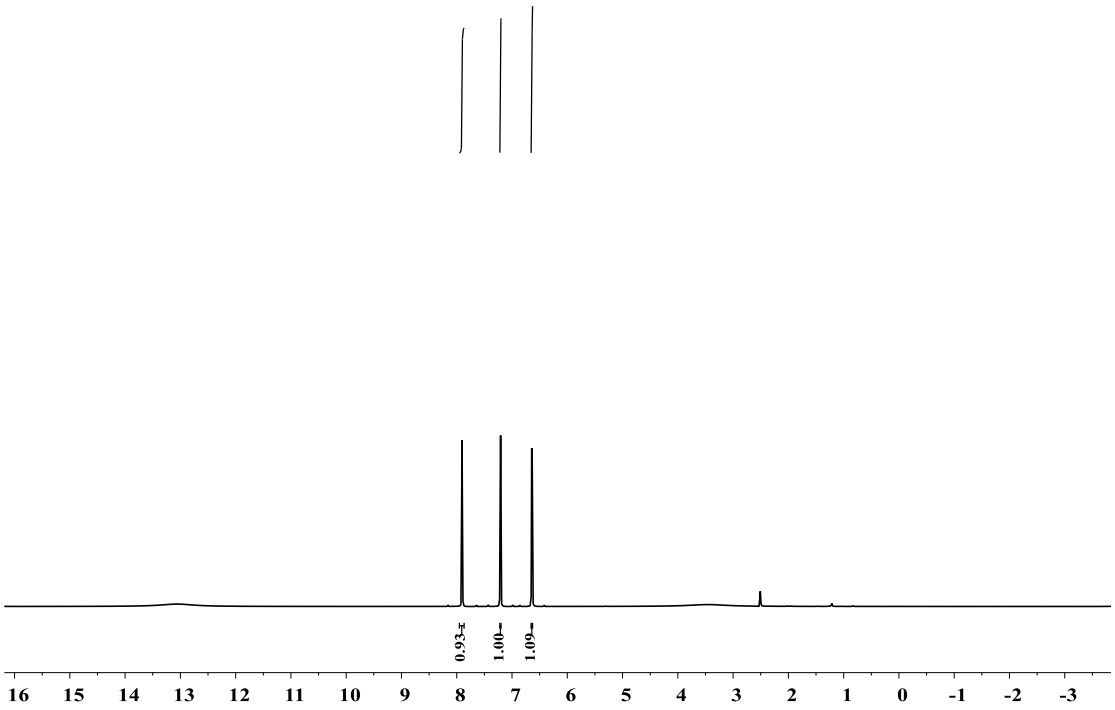

Figure S35. ^{1}H NMR spectra of 2-furoic acid.

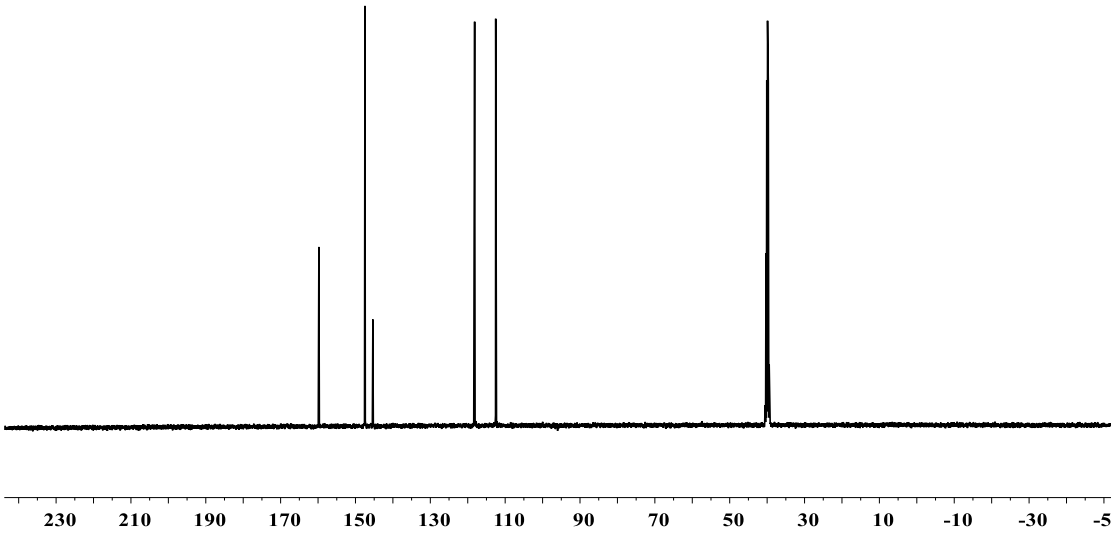

Figure S36. ^{13}C NMR spectra of 2-furoic acid.

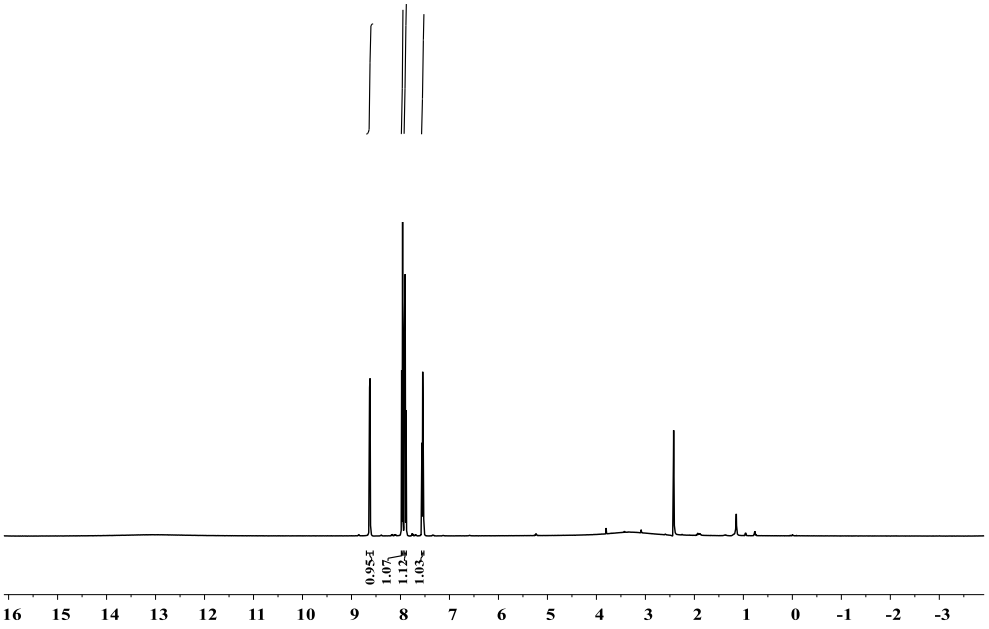

Figure S37. ^{1}H NMR spectra of 2-picolinic acid.

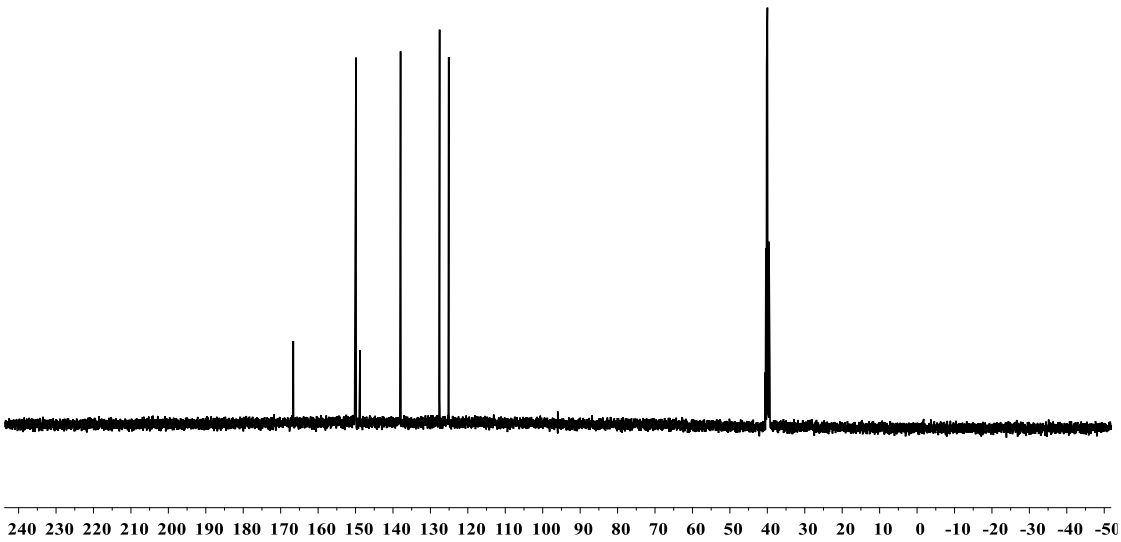

Figure S38. ^{13}C NMR spectra of 2-picolinic acid.

To confirm the proposed free radical reaction mechanism, excess butylated hydroxytoluene (BHT), a radical scavenger, was added into the reaction system at 8 h. As is shown in Figure S39, the reaction stopped with the benzaldehyde conversion rate of 68%, indicating a free radical reaction mechanism of (CAAC)Cu catalyzed aerobic oxidation.

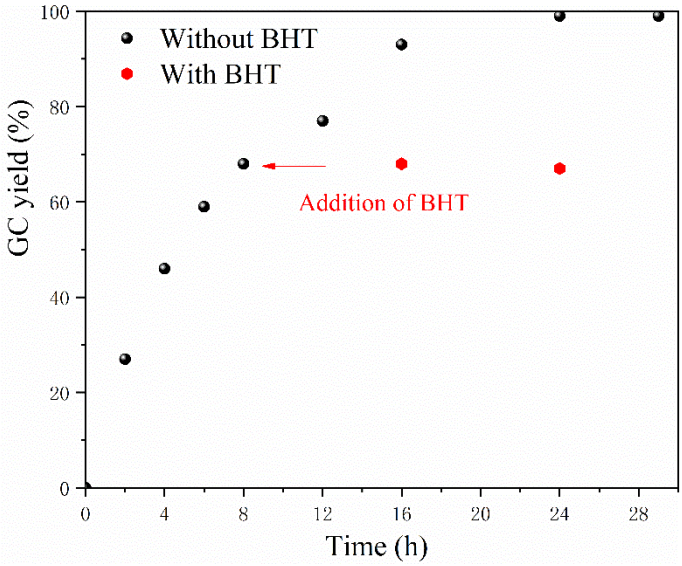

Figure S39. Kinetic study of aerobic oxidation of benzaldehyde under mild condition.

Reference

(S1) Frisch, M. J.; Trucks, G. W.; Schlegel, H. B.; Scuseria, G. E.; Robb, M. A.; Cheeseman, J. R.; Montgomery, Jr., J. A.; Vreven, T.; Kudin, K. N.; Burant, J. C.; Millam, J. M.; Iyengar, S. S.; Tomasi, J.; Barone, V.; Mennucci, B.; Cossi, M.; Scalmani, G.; Rega, N.; Petersson, G. A.; Nakatsuji, H.; Hada, M.; Ehara, M.; Toyota, K.; Fukuda, R.; Hasegawa, J.; Ishida, M.; Nakajima, T.; Honda, Y.; Kitao, O.; Nakai, H.; Klene, M.; Li, X.; Knox, J. E.; Hratchian, H. P.; Cross, J. B.; Adamo, C.; Jaramillo, J.; Gomperts, R.; Stratmann, R. E.; Yazyev, O.; Austin, A. J.; Cammi, R.; Pomelli, C.; Ochterski, J. W.; Ayala, P. Y.; Morokuma, K.; Voth, G. A.; Salvador, P.; Dannenberg, J. J.; Zakrzewski,

V. G.; Dapprich, S.; Daniels, A. D.; Strain, M. C.; Farkas, O.; Malick, D. K.; Rabuck, A. D.; Raghavachari, K.; Foresman, J. B.; Ortiz, J. V.; Cui, Q.; Baboul, A. G.; Clifford, S.; Cioslowski, J.; Stefanov, B. B.; Liu, G.; Liashenko, A.; Piskorz, P.; Komaromi, I.; Martin, R. L.; Fox, D. J.; Keith, T.; Al-Laham, M. A.; Peng, C. Y.; Nanayakkara, A.; Challacombe, M.; Gill, P. M. W.; Johnson, B.; Chen, W.; Wong, M. W.; Gonzalez, C.; and Pople, J. A.; Gaussian, Inc., Pittsburgh PA, **2009**.